

How clay mineral assemblages affect instability on the upper slope of the Hikurangi subduction zone, New Zealand

Michael Underwood¹, Brandon Dugan², and Sebastian Cardona³

¹New Mexico Institute of Mining and Technology

²Colorado School of Mines

³Texas A&M University

November 24, 2022

Abstract

The International Ocean Discovery Program cored Sites U1517 (Tuaheni landslide complex) and U1519 (upper Tuaheni Basin) on the Hikurangi margin, North Island, New Zealand. Strong ocean currents result in unusual amounts of compositional homogeneity in the muds. Detrital smectite dominates among clay minerals, with average proportions of 52 wt% at Site U1517 and 53 wt% at Site U1519. Bulk sediment from Site U1517 contains up to ~29 wt% smectite (average = 21 wt%), high enough to reduce the angle of internal friction (on average) to ~6°. There are no compositional excursions along inferred slip surfaces or weak layers. Smectite decreases toward the SW in the “downstream” direction of the East Cape Current, and that spatial trend correlates with lower densities of slide scars.

25 **Abstract**

26 The International Ocean Discovery Program cored Sites U1517 (Tuaheni landslide complex) and U1519
27 (upper Tuaheni Basin) on the Hikurangi margin, North Island, New Zealand. Strong ocean currents result in
28 unusual amounts of compositional homogeneity in the muds. Detrital smectite dominates among clay minerals,
29 with average proportions of 52 wt% at Site U1517 and 53 wt% at Site U1519. Bulk sediment from Site U1517
30 contains up to ~29 wt% smectite (average = 21 wt%), high enough to reduce the angle of internal friction (on
31 average) to ~6°. There are no compositional excursions along inferred slip surfaces or weak layers. Smectite
32 decreases toward the SW in the “downstream” direction of the East Cape Current, and that spatial trend
33 correlates with lower densities of slide scars.

34 **Plain Language Summary**

35 Expandable clay minerals of the smectite group are notorious for weakening soils and marine sediments and
36 contributing to conditions that promote landslides. The Hikurangi margin offshore North Island, New Zealand,
37 is noted for its abundance of submarine landslides. To assess their possible causes, we analyzed clay mineral
38 assemblages from two sites on the upper trench slope that were sampled by the International Ocean Discovery
39 Program (Sites U1517 and U1519). Cores from both sites display unusual degrees of compositional homogeneity,
40 with smectite as the dominant clay mineral. Illite occurs in lesser amounts, and the concentrations of chlorite
41 and kaolinite are relatively minor. Cores from Site U1517 encompass the Tuaheni landslide complex, but we
42 did not find any compositional anomalies at inferred slip surfaces or along weak layers. Instead, the entire
43 stratigraphic succession appears to be relatively weak. Because of that inherited preconditioning, dynamic
44 loading during such events as large earthquakes is probably enough to trigger numerous submarine landslides.
45 However, there appears to be no predisposition for slip along any unusually weak, layer-specific interval of the
46 sediment.

47 **1 Introduction**

48 Sedimentary facies in active subduction zones with high rates of terrigenous sedimentation (e.g., Cascadia,
49 Nankai Trough, southern Chile Trench, Sumatra, Makran) are governed by interactions among eustasy,
50 tectonics, and sediment-transport processes (e.g., Piper et al., 1973; Underwood & Bachman, 1982; Thornburg
51 & Kulm, 1987). Subduction accretion normally creates a stair-step series of intraslope basins separated by
52 fault-cored anticlinal ridges (e.g., Moore & Karig, 1976; McAdoo et al., 2004; Ding et al., 2010; Contardo et
53 al., 2011). Some unconfined flows are capable of overtopping bathymetric highs (Muck & Underwood, 1990),
54 but taller ridges tend to block such pathways. Consequently, slope basins behind taller tectonic ridges typically
55 act as traps for turbidity currents, slumps, mudflows, and debris-flows (e.g., Moore & Karig, 1976; Underwood
56 & Moore, 1995; Contardo et al., 2008; Nelson et al., 2011), whereas steeper slopes are usually covered by mud
57 that settles slowly from suspension.

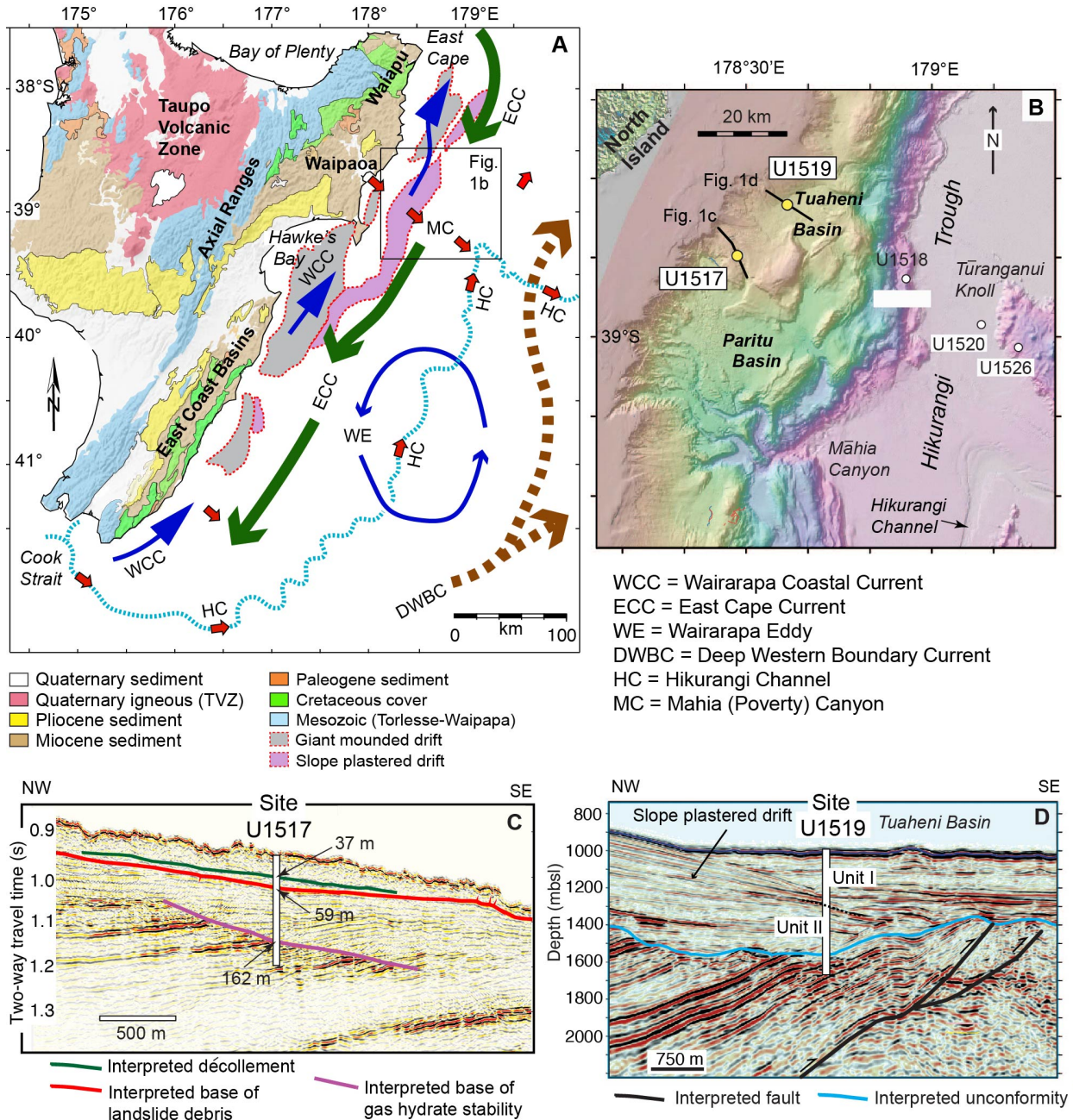
58 Submarine slides are common in subduction zones (e.g., Yamada et al., 2010; Harders et al., 2011; Hill et al.,
59 2020), but their spatial distributions are challenging to understand, and their triggering mechanisms are often
60 impossible to pin-point. Geotechnical tests provide clues by revealing how frictional properties change with
61 concentrations of individual minerals (e.g., Lupini et al., 1981; Shimamoto & Logan, 1981; Logan &
62 Rauenzahn, 1987; Tiwari & Marui, 2005; Tembe et al., 2010; Ikari et al., 2018). Many additional variables
63 need to be considered, however: seafloor topography; rates of sediment accumulation; grain size distribution,
64 especially the proportion of clay-sized grains; particle shape and microfabric; hydration state of clay minerals;
65 porosity, permeability, and pore-fluid pressure; consolidation and lithification; and dynamic loading by
66 earthquakes (e.g., Hampton et al., 1996; Locat & Lee, 2002; Masson et al., 2006; Bartetzko & Kopf, 2007;
67 Ikari et al., 2007, 2011; Kock & Huhn, 2007; Saffer & Tobin, 2011; Takahashi et al., 2014; Trutner et al.,
68 2015; Kremer et al., 2017; Silver & Dugan, 2020). Those variables seemingly combine in ways that are unique
69 to each individual locale (Vanneste et al., 2014).

70

71 The Hikurangi margin offshore North Island, New Zealand (Fig. 1a) conforms to most of the paradigms of
72 subduction-zone tectonics and sedimentation (Bostock et al., 2018). The margin's architecture includes forearc
73 basins, imbricate thrusts and folds within the frontal accretionary prism, and scattered slope basins (e.g.,
74 Tuaheni Basin) (Barnes et al., 2002; Paquet et al., 2009; Pedley et al., 2010; Poudoux et al., 2012; Ghisetti et
75 al., 2016). The landward trench slope is also noteworthy for submarine landslides, including the Tuaheni
76 landslide complex (Collot et al., 2001; Mountjoy et al., 2014b; Watson et al., 2020). Hikurangi deviates from
77 the global paradigm, however, in two important ways: ocean currents are strong, and contourite drifts and
78 hybrid contourites are widespread (Bailey et al., 2020, 2021; Couvin et al., 2020). Mindful of those facts, we
79 focus attention in this paper on how slope-parallel currents affect mud composition across the mid to upper
80 slope. We test whether that composition has had any demonstrable influence on slope stability and landslides.
81 Our results for Hikurangi provide a tightly constrained case study that serves as a benchmark for comparisons
82 of cause-and-effect for slope failures and mass-transport deposits along other margins.

83

84 Dispersal and deposition of fine-grained suspended sediment in the oceans are governed by several processes
85 (e.g., Gorsline, 1984; McCave, 1984). Sediment gravity flow provides one mechanism for directing mud onto
86 the Hikurangi slope, as unconfined turbidity currents and/or by funneling through submarine canyons
87 (Mountjoy et al., 2009a, 2014a; Alexander et al., 2010; Poudoux et al., 2012). Margin-parallel ocean currents
88 provide the main competition (Carter & Wilkin, 1999; Chiswell et al., 2015). The NE-directed Wairarapa
89 Coastal Current (Fig. 1a) carries suspensions along the continental shelf and uppermost slope (Foster & Carter,
90 1997; Chiswell, 2000). A strong SW-directed current (East Cape Current) dominates the mid to upper slope
91 (Fig. 1a), extending to a water depth of ~1300 m (Chiswell & Roemmich, 1998). Transient counterclockwise
92 gyres (e.g., Wairarapa Eddy) impact surface-water farther offshore (Fig. 1a), but their temporal stability



93
94
95
96
97
98
99
100
101
102

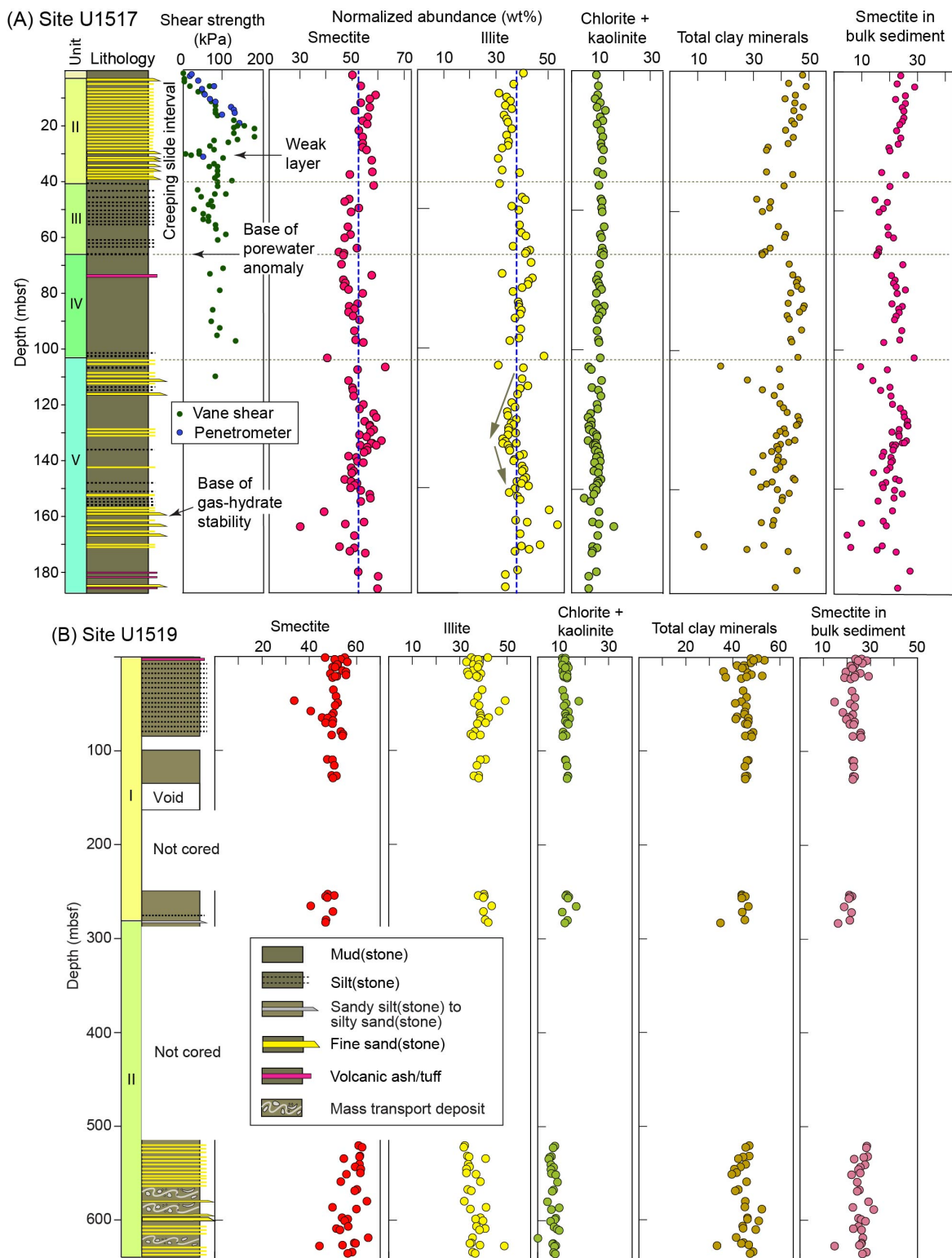
Figure 1. a. Simplified map of onshore geology, North Island, New Zealand (modified from Jiao et al., 2014), prominent bathymetric features, ocean currents, and pathways for sediment transport by gravity flow. Giant mounded drifts and slope plastered drifts from Bailey et al. (2020). b. Bathymetric map with locations of Tuaheni Basin and IODP sites (from Saffer et al., 2017). c. Seismic reflection profile crossing IODP Site U1517. Interpretations from Barnes et al. (2019a). d. Seismic reflection profile crossing IODP Site U1519. Interpretation of slope plastered drift from Bailey et al. (2020). Interpretations of faults and unconformity from Barnes et al. (2019b). See Fig. 1b for tracklines.

103 and maximum water depths remain uncertain (Chiswell & Roemmich, 1998; Chiswell, 2005). Seaward of the
104 trench, the Deep Western Boundary Current (Fig. 1a) dominates abyssal circulation and drift sedimentation
105 (Carter & McCave, 1997, 2002; Carter et al., 2004). Those currents set up a likelihood of persistent mixing of
106 suspensions from downslope versus along-slope routing.

107
108 The International Ocean Discovery Program (IODP) positioned Site U1519 in Tuaheni Basin on the upper
109 trench slope (Fig. 1b), approximately 38 km from shore at a water depth of 1000 m. The site lies well within
110 the domain of the East Cape Current (Fig. 1a), and Bailey et al. (2020, 2021) recognized the nearby acoustic
111 character as a “slope plastered” contourite drift (Fig. 1c). Shipboard sedimentologists (Barnes et al., 2019b)
112 defined two lithostratigraphic units (Fig. 2b). Unit I (0–282.66 mbsf) is composed of mud and mudstone with
113 sparse and very thin interbeds of silt and volcanic ash (Fig. 2b), whereas unit II (282.66–635.65 mbsf) consists
114 of mudstone with scattered interbeds of siltstone, sandy siltstone, and sandstone (inferred turbidites). Some
115 intervals display convolute laminae, mesoscale folds, dismembered bedding, and clasts of mudstone in a
116 mudstone matrix, all suggestive of mass transport. Evidence from cores for contourite deposition is
117 inconclusive. In general, diagnostic criteria remain elusive for distinguishing among turbidites, contourites,
118 hemipelagites, and hybrids (Stow et al., 2002; Stow & Smillie, 2020). Definitive bed-by-bed identification
119 requires time-consuming post-cruise analyses of microstructures, ichnofacies, grain size distributions,
120 mineralogy, geochemistry, and/or computed tomography (e.g., Alonso et al., 2016; Nishida, 2016; Rodriguez-
121 Tovar & Hernandez-Molina, 2018; Vandorpe et al., 2019; de Castro et al., 2020). Unfortunately, rigorous
122 analyses of the cores from Site U1519 were thwarted by wide gaps between intervals of core (Fig. 3b),
123 unusually poor recovery (~55%), and widespread (severe) drilling disturbance. Thus, the prevalence of
124 contourites near Site U1519 is based largely on seismic-reflection interpretations (Bailey et al., 2020).

125
126 At a water depth of ~732 m (Fig. 1b), Site U1517 is also well within the core of the East Cape Current
127 (Chiswell et al., 2015), and seismic-reflection data are indicative of a “slope plastered” contourite drift (Bailey
128 et al., 2020, 2021). The primary purpose of drilling Site U1517, however, was to log and sample through the
129 Tuaheni landslide complex (Mountjoy et al., 2014b). Creep seems to have occurred where the base of gas-
130 hydrate stability pinches out at the seafloor (Mountjoy et al., 2009b, 2014b), so one hypothesis is that
131 occlusion of permeability by gas hydrate may have led to overpressured conditions and hydrofracturing
132 (Crutchley et al., 2010; Ellis et al., 2010; Gross et al., 2018). Hydrate-bearing sediments, moreover, might be
133 prone to time-dependent plastic deformation (Mountjoy et al., 2014b). To test those ideas, the cored interval at
134 Site U1517 (Fig. 1d) crossed interpreted positions of the décollement at ~37 mbsf, the base of landslide debris
135 at ~59 mbsf, and the base of gas-hydrate stability at ~162 mbsf (Barnes et al., 2019a).

136
137 According to shipboard scientists (Barnes et al., 2019a), unit I at Site U1517 (0–3.0 mbsf) consists of a thin
138 Holocene mud blanket (Fig. 2a). Unit II (3.0–40.74 mbsf) contains interbeds of mud and very fine sand. The



139

140

141 Figure 2. a. XRD results for IODP Site U1517 (Underwood and Dugan, 2021). Proportions of total clay minerals
 142 and values of shear strength from Barnes et al. (2019a). b. XRD results for IODP Site U1519 (Underwood 2022).
 143 Proportions of total clay minerals from Barnes et al. (2019b).

144 bioturbated mud within unit III (40.74–66.38 mbsf) alternates with laminated stacked couplets of silt and clay,
145 resembling silty contourites described elsewhere (e.g., Stow et al., 2002; Stow & Smillie, 2020). Unit IV
146 (66.38–103.16 mbsf) consists mostly of structureless mud, whereas unit V (103.16–187.53 mbsf) contains
147 numerous interbeds of normally graded sand (inferred turbidites) and mud (Fig. 2a). Barnes et al. (2019a)
148 provisionally assigned the upper ~67 m of strata to the Tuaheni landslide complex (Fig. 2a), but many
149 questions about the landslide remain. Gas hydrate was detected, for example, but only at depths deeper than
150 100 mbsf (Barnes et al., 2019a); that observation and numerical modeling indicate that gas-hydrate dynamics
151 are unlikely as the main destabilizing variable (Screaton et al., 2019). Couvin et al. (2020) identified two
152 chaotic acoustic intervals in nearby seismic-reflection profiles, but the correlative intervals of core (units II and
153 III) are perplexing because they display almost no internal deformation; moreover, there are no mesoscopic
154 indicators of concentrated slip at the base of the inferred landslide (Barnes et al., 2019a). The only core-scale
155 indicators of gravity-driven, soft-sediment deformation are scattered patches that display convolute bedding
156 and/or intraformational mud clasts (Barnes et al., 2019a). Couvin et al. (2020) suggested that Hole U1517C
157 intersected an intact block within an otherwise chaotic landslide. Adding to the debate, Luo et al. (2020) used
158 numerical modeling of porewater-chemistry data to support their contention of two slip events. The more-
159 recent failure evidently occurred as a coherent 40-m-thick block, which places the décollement at the base of
160 unit II. On the other hand, shipboard measurements of shear strength (Barnes et al., 2019a) revealed a weak
161 interval centered at ~31 mbsf, within the middle of unit II (Fig. 2a). These conflicting results and
162 interpretations deserve more scrutiny. Our objective here is to determine if excursions in clay mineralogy
163 might be large enough to have affected the sediment's shear strength along any slip surfaces or weak intervals.

164

165 **2 Materials and Methods**

166 Samples from Sites U1517 and U1519 were positioned with several collocated subsamples (“clusters”) adjacent to
167 whole rounds that had already been extracted from cores for tests of interstitial water chemistry and geotechnical/
168 frictional/hydrogeologic properties. Coarser interbeds were avoided. See Underwood and Dugan (2021) for detailed
169 descriptions of sample preparation and XRD methods. To reiterate briefly, mud specimens were disaggregated, and
170 oriented aggregates of glycol-saturated clay-sized splits (<2 μm equivalent spherical settling diameter) were
171 prepared using the filter-peel method (Moore & Reynolds, 1989). XRD scans were completed using a Panalytical
172 X'Pert Pro diffractometer, and values of normalized relative mineral abundance were computed using a set of
173 regression equations that relate wt% values to peak area. Absolute errors of accuracy are: illite = 3.0 wt%, smectite
174 = 3.9 wt%, and undifferentiated (chlorite + kaolinite) = 5.1 wt% (Underwood et al., 2020). Compositional
175 differences among individual specimens, or between lithologic units, are not regarded as geologically significant
176 unless they exceed those errors.

177 **3 Data**

178 The cored intervals at Site U1519 display unusually small amounts of compositional scatter, with minor (but
179 statistically significant) differences between the two lithologic units (Fig. 3b). Results of 76 measurements
180 (Underwood, 2021) show smectite to be the most abundant clay mineral (site average = 53 wt%), with
181 normalized abundances ranging from 33 to 65 wt%. Proportions of illite range from 32 to 49 wt%, and the
182 values for undifferentiated (chlorite + kaolinite) are 0–16 wt%. The mean (μ) and standard deviation (σ) values
183 for unit I are smectite: $\mu = 50$ wt%, $\sigma = 4$; illite: $\mu = 38$ wt%, $\sigma = 3$; and undifferentiated (chlorite + kaolinite):
184 $\mu = 12$ wt%, $\sigma = 1$. Comparable statistics for unit II are smectite: $\mu = 57$ wt%, $\sigma = 5$; illite: $\mu = 36$ wt%, $\sigma = 4$;
185 undifferentiated (chlorite + kaolinite): $\mu = 7$ wt%, $\sigma = 2$.

186
187 The ninety-nine specimens from Site U1517 (Underwood & Dugan, 2021) likewise reveal small variations
188 among the five lithologic units (Fig. 2a). Smectite is the most abundant clay mineral (site average = 52 wt%),
189 with a range of 30–63 wt% (Fig. 2a). Percentages of illite range from 31 to 54 wt%, and the range for
190 undifferentiated (chlorite + kaolinite) is 5–16 wt%. The mean and standard deviation statistics for unit II are
191 smectite: $\mu = 55$ wt%, $\sigma = 3$; illite: $\mu = 34$ wt%, $\sigma = 2$; undifferentiated (chlorite + kaolinite): $\mu = 11$ wt%, $\sigma =$
192 1. Values for unit III are smectite: $\mu = 48$ wt%, $\sigma = 2$; illite: $\mu = 40$ wt%, $\sigma = 2$; chlorite + kaolinite: $\mu = 11$
193 wt%, $\sigma = 0.5$. Statistics for unit IV are smectite: $\mu = 51$ wt%, $\sigma = 5$; illite: $\mu = 39$ wt%, $\sigma = 4$; undifferentiated
194 (chlorite + kaolinite): $\mu = 10$ wt%, $\sigma = 1$. In unit V, the statistics are smectite: $\mu = 53$ wt%, $\sigma = 5$; illite: $\mu = 38$
195 wt%, $\sigma = 4$; undifferentiated (chlorite + kaolinite): $\mu = 9$ wt%, $\sigma = 2$. Unit V displays the greatest amount of
196 statistical scatter, with subtle gradients of decreasing, then increasing proportions of illite moving down-
197 section (Fig. 2a). Compositional shifts at horizons of interest (e.g., ~31, ~41, ~66 mbsf) are trivial, however,
198 and within the normal error range for the method (Fig. 2a).

199
200 Concentrations of individual minerals in bulk sediment are more diagnostic if the goal is to assess how
201 composition affects hydrogeological, frictional, and geotechnical properties. The average content of total clay
202 minerals at Site U1517 is 40 wt%, with a range of 10–49 wt% (Barnes et al., 2019a). Average values for bulk
203 sediment are: smectite = 1 wt% ($\sigma = 4$); illite = 15 wt% ($\sigma = 3$); and undifferentiated (chlorite + kaolinite) = 4
204 wt% ($\sigma = 0.9$). Contrasts across unit boundaries are within the background range of scatter, and excursions are
205 absent at the suspected slip surfaces (Fig. 2a). Data from Site U1519 are similar (Fig. 2b).

206 To expand spatial coverage, we also collected data from 30 specimens from piston and gravity cores
207 (Underwood, 2020), from the vicinity of the Ruatoria debris avalanche in the NE to offshore Hawke's Bay in
208 the SW (Fig. 3a). Smectite ranges from 29 to 54 wt% ($\mu = 45$, wt% $\sigma = 6$). The range for illite is 36–57 wt% (μ
209 = 43 wt%, $\sigma = 5$), and undifferentiated (chlorite + kaolinite) ranges from 9 to 16 wt% ($\mu = 12$ wt%, $\sigma = 2$).
210 These values overlap data from Sites U1517 and U1519, but with more statistical scatter. Moreover, samples

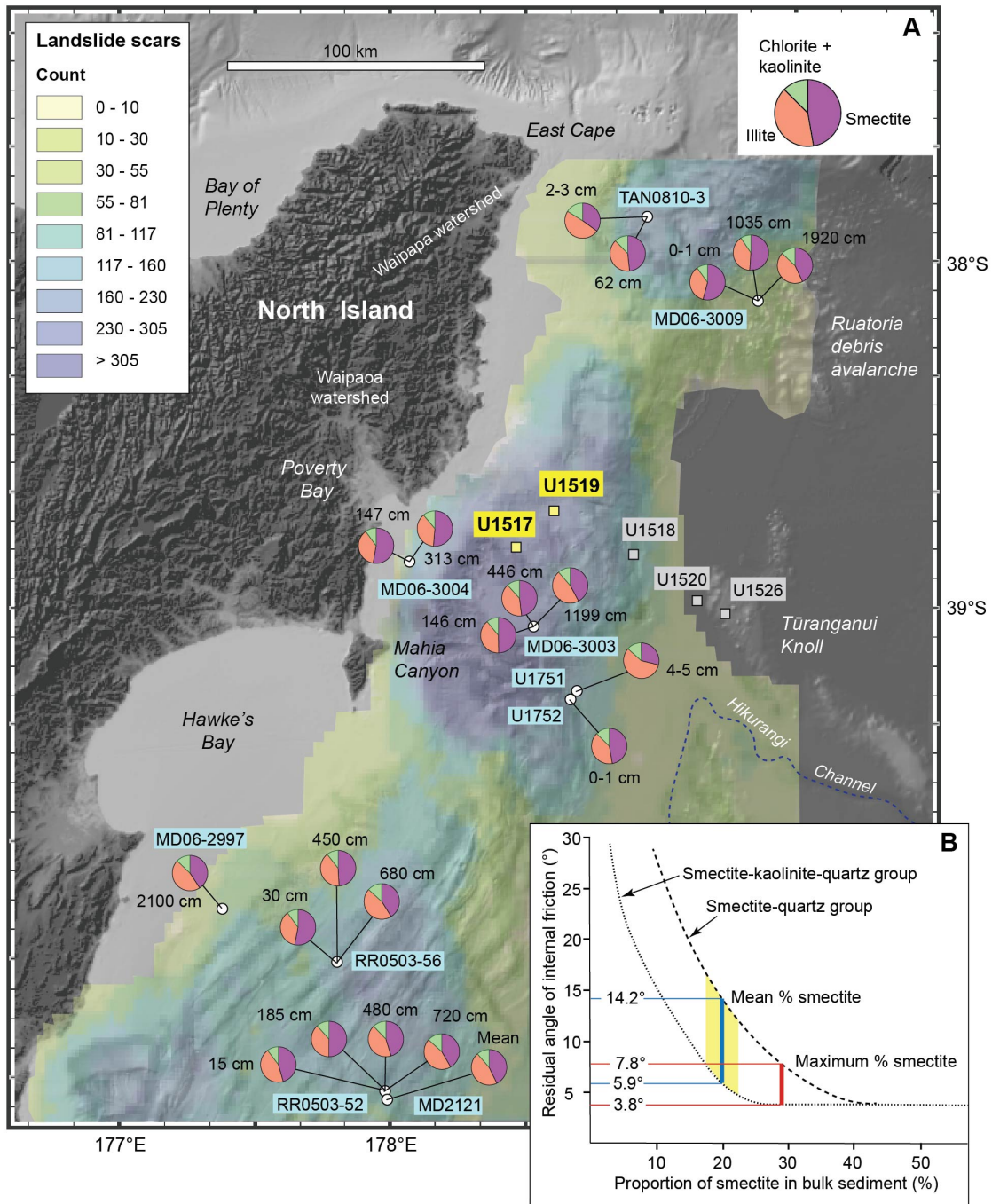
211 from the NE corner of the study area generally contain more smectite (and less illite) compared to those to the
212 SW (Fig. 3a).

213 **4 Results**

214 4.1. Principal Sources for Detrital Clays

215 If our results are viewed in the context of geotechnical inquiry, it doesn't really matter where the clays
216 originated, or how they arrived at sites of deposition, but we offer some possibilities. Illite is the expected
217 weathering product of plutonic, low-grade metasedimentary, and sedimentary sources (Biscaye, 1965; Fagel,
218 2007). Basement rocks across New Zealand (Fig. 1a) consist mostly of illite- and chlorite-rich metagraywackes
219 and argillites of the Torlesse and Waipapa terranes (Sporli, 1978; MacKinnon, 1983; Warr & Cox, 2016).
220 Younger cover sequences and forearc deposits in the East Coast Basin, and in regions immediately southeast of
221 the Axial Range (Fig. 1a), are composed of moderately indurated illite-rich sedimentary strata with scattered
222 tuff and bentonitic marl (e.g., Neef, 1999; Browne, 2004; Maison et al., 2018; McArthur et al., 2020). Rivers in
223 the area (e.g., the Waipaoa River, Fig. 1a) erode into poorly indurated Miocene-Pliocene sediments (Erdman &
224 Kelsey, 1992; Reid, 1998; Browne, 2004; Marsaglia et al., 2010). Although smectite is also a reported
225 constituent of the mudstones (Claridge, 1960), illite is the dominate clay in soil samples from steep-land fields
226 (Officer et al., 2006). Those watersheds (e.g., Waipaoa) generate unusually high yields of suspended sediment
227 (Hicks et al., 2011), and discharge should supply the Hikurangi shelf and slope with illite-rich clays.

228
229 Sedimentologists usually attribute high concentrations of smectite to weathering or alteration of volcanic
230 sources (Biscaye, 1965; Hein & Scholl, 1978; Fagel, 2007; Huff, 2016). The East Cape region of North Island
231 (Fig. 1) exposes several potential parents for detrital smectite. Mafic *mélange* (disrupted ophiolite) and small
232 lenses of volcanic conglomerate do exist in the East Coast Allochthon (Brothers & Delaloye, 1982; Cluzel et
233 al., 2010; Marsaglia et al., 2014), but their exposures are probably not large enough to produce all the smectite
234 we found in the slope muds. The Taupo Volcanic Zone (TVZ), on the other hand, fits all the prerequisites for a
235 regionally extensive source (Fig. 1a), with enormous andesitic to rhyolitic calderas (Kohn & Topping, 1978;
236 Cole et al., 2014; Wilson & Rowland, 2016), ignimbrites, tephra, and lahars (e.g., Cronin et al., 1999;
237 Hidgson & Manville, 1999; Lowe et al., 2013; Downs et al., 2014; Procter et al., 2014; Gravley et al., 2016).
238 Their chemical weathering products are demonstrably smectite-dominant, and those clays are ubiquitous in
239 geothermal and hydrothermal systems (Libbey et al., 2013; Simpson et al., 2019; Heap et al., 2020). After
240 reaching the Bay of Plenty coast, at least some particulates from the TVZ are likely swept eastward by the East
241 Cape Current before that current bifurcates around East Cape and directs suspensions toward the SW (Fig. 1a).
242 Moreover, heavily weathered tephra is widespread in coastal exposures around the Bay of Plenty (Iso et al.,
243 1982), and smectite alteration of volcanoclastic sediment permeates into geothermal systems offshore (Hocking
244 et al., 2010). Farther to the east near East Cape, discharge from the Waiapu River is known to contain
245 remarkably high loads of suspended sediment (Hicks et al., 2011); that discharge might contribute some



246
 247 Figure 3a. Locations of piston-gravity cores used in this study, with depths of specimens in cm below seafloor
 248 (Underwood, 2020). Pie diagrams depict normalized proportions of smectite, illite, and undifferentiated (chlorite +
 249 kaolinite). Background shows frequency distribution of landslide scars (from Watson et al., 2020). 3b. Empirical
 250 relation between proportion of smectite in bulk sediment and residual angle of internal friction, as determined by
 251 Tiwari & Marui (2005). Average and maximum values for Site U1517 yield predictions for the Tuaheni landslide.
 252 Yellow field depicts one standard deviation around the mean.

253
 254 additional smectite into suspensions carried by the East Cape Current, but also higher concentrations of illite
 255 and chlorite liberated from easily eroded sedimentary strata. We suggest that the typical Hikurangi clay

256 mineral assemblage, with appreciable amounts of both smectite and illite, is a product of blending among
257 suspensions from multiple sources along the pathway of the East Cape Current.

258 4.2. Implications for Slope Stability

259 It seems certain that several factors combine to destabilize the Hikurangi trench slope, but it is challenging to
260 isolate and quantify the impact of each. Rapid accumulation of low-permeability sediments often contributes to
261 overpressured conditions on continental slopes (e.g., Stoecklin et al., 2017). Contourite drifts elsewhere are
262 known to be susceptible to failure due to such factors as localized oversteepening of the seafloor, scouring by
263 currents, and/or pronounced climate-induced changes of lithology (e.g., Laberg et al., 2016; Prieto et al., 2016;
264 Miramontes et al., 2018; Gatter et al., 2020). Fluid pressures in such deposits can be exacerbated by trapping or
265 seepage of free gas (e.g., Faure et al., 2006; Gross et al., 2018; Crutchley et al., 2022). The Hikurangi margin,
266 in addition, has a propensity for moderate to large subduction-induced earthquakes (Dowrick & Rhoades,
267 1998; Cubrinovski et al., 2022), so it is also logical to expect dynamic loading during seismic shaking, together
268 with transient increases of fluid pressure (e.g., Stegmann et al., 2007). The Ruatoria avalanche offshore North
269 Island has been attributed to seamount subduction (Collot et al., 2001; Lewis et al., 2004). No matter how
270 sedimentologists might debate interpretations of detrital provenance and routing paths for any depositional
271 system, the abundance of clay and the composition of clay minerals also play key roles in modulating
272 sediment's frictional strength. Smectite is widely regarded as a crucial ingredient in that sense (Tembe et al.,
273 2010). Residual shear strength decreases dramatically once the proportion of smectite exceeds 25–30% of the
274 bulk mineralogy (e.g., Luipini et al., 1981; Logan & Rauenzahn, 1987). The results of Tiwari & Marui (2005)
275 allow us to predict ranges of residual shear strength for the Tuaheni landslide based on our calculated
276 percentages of smectite in the bulk sediment. Using the empirical relation for two-component quartz-smectite
277 mixtures, those %-smectite values translate to predicted angles of internal friction that range from an average
278 of 14.2° to a minimum of 7.8° (Fig. 3b). The three-component quartz-smectite-kaolinite group (Tiwari &
279 Marui, 2005) provides a more realistic match for Hikurangi bulk sediment. Using that curve, our calculated
280 values for bulk %-smectite translate to predictions of 5.9° for the average and only 3.8° for the minimum angle
281 of internal friction (Fig. 3b). Accordingly, although direct tests of frictional property are warranted to verify,
282 we stipulate that clay composition preconditions the Tuaheni strata to fail without having a preferred slip
283 surface along any layer-specific weak interval.

284
285 Crutchley et al. (2022) contended that the basal shear zone of the Tuaheni slide exploited a stratigraphic
286 interval with comparatively low shear strength (i.e., a pre-existing weak layer). Weak layers are known to
287 occur in many lithologies (Gatter et al., 2021). Some weak layers evidently predate failure and function as the
288 preferred glide planes, whereas others form during failure events due to realignment of grain fabric (Locat et
289 al., 2014; Gatter et al., 2021). In some instances, contrasts of hydrogeologic properties across a pronounced
290 lithologic boundary allow pore pressure to build up along a potential failure plane (e.g., Stegmann et al., 2007).

291 Elsewhere, tephra beds act as weak layers; their suggested causes include fabric rearrangement and volume
292 reduction during shearing (Harders et al., 2010), alteration of the volcanic glass to smectite (Miramontes et al.,
293 2018), or the tephra's role in focusing transient perturbations of pore-fluid pressure (Wiemer et al., 2015;
294 Kuhlmann et al., 2016). Our data allow for tests of those possibilities.

295
296 Surprisingly, we found no evidence at Site U1517 for pronounced compositional variations within or across
297 any of the weak layers or inferred slip surfaces. Compositional homogeneity prevails across the slip surface at
298 ~41 mbsf, across the base of the creeping slide interval (as defined by seismic-reflection data at ~59 mbsf), and
299 within the weak layer at ~31 mbsf (Fig. 2a). None of those intervals in the cores coincides with a layer of
300 volcanic ash, or unusually high amounts of total clay, or unusually high concentrations of smectite (Fig. 3a).
301 Instead, we see a subtle facies transition between mud with stacked couplets of silt and mud (unit III) and
302 mostly mud (unit IV). That facies change probably resulted from temporal variations in sediment supplies and
303 current strength. The weak layer at ~31 mbsf occurs in the middle of unit III, without any obvious facies
304 change or anomaly in sediment texture, internal sedimentary structures, bed thickness, or bed geometry (Fig.
305 2a). That weak layer probably developed during a slip event via realignment of phyllosilicate grain fabric
306 (Crutchley et al., 2022).

307
308 If we accept the validity of the East Cape Current as the path for routing residual smectite toward the SW, then
309 it follows for slope stability offshore North Island to improve “downstream” where more detrital illite and
310 chlorite enters the dispersal system from the Waipaoa and kindred watersheds (Fig. 1a). XRD data from
311 piston/gravity cores are consistent with that interpretation (Fig. 3a). The frequency of landslide scars decreases
312 where proportions of illite and chlorite are higher (Watson et al., 2020). In the opposite direction, landslide
313 scars are more concentrated in areas that are closer to the volcanic sources of smectite-rich clay (Fig. 3a).

314 **5 Conclusions**

315 Our results reinforce the notion that submarine slopes fail in response to many interwoven variables, including
316 mineralogy, and those variables combine in ways that are unique to each individual landslide. The homogeneity
317 of mud across the Hikurangi trench slope is a result of strong currents blending suspensions from multiple
318 sources. Smectite is the most abundant clay mineral, with concentrations high enough to reduce the bulk mud's
319 angle of internal friction to an average of ~6° and a minimum of ~4°. We did not find compositional
320 excursions along any inferred slip surfaces or weak layers within the Tuaheni landslide. Smectite abundance
321 and slide scars both decrease toward the SW, in the “downstream” direction of the East Cape Current. Thus,
322 sediment-dispersal systems such as Hikurangi can contribute inconspicuously to strike-parallel changes in
323 slope instability by modulating composition. Our study demonstrates why quantitative analyses of mineralogy

324 should be included in any holistic investigation of landslides, to test for possible compositional
325 preconditioning.

326 **Acknowledgments**

327 This study used samples provided by the International Ocean Discovery Program (IODP) and core repositories
328 at Lamont-Doherty Earth Observatory, Oregon State University (supported by NSF Grant number OCE-
329 1558679), and the New Zealand National Institute of Water and Atmospheric Research. Funding was provided
330 by the U.S. Science Support Program and, for piston/gravity cores, by a grant to Laura Wallace at GNS
331 Science of New Zealand. We thank the crew members on JOIDES Resolution, IODP technicians, and fellow
332 shipboard scientists for assisting with sample acquisition. Karissa Rosenberger and Mercedes Salazar helped
333 with sample preparation, and Kelsey McNamara completed XRD scans at the New Mexico Bureau of Geology
334 and Mineral Resources.

335

336 **Open Research**

337 Tabulations of XRD data, descriptions of methods, and error analysis are accessible in data reports distributed
338 by the International Ocean Discovery Program: <https://doi.org/10.14379/iodp.proc.372B375.201.2020>;
339 <https://doi.org/10.14379/iodp.proc.372B375.203.2020>; <https://doi.org/10.14379/iodp.proc.372B375.209.2022>;
340 <https://doi.org/10.14379/iodp.proc.372A.201.2021>

341

342 **References**

- 343 Alexander, C. R., Walsh, J. P., & Orpin, A. R. (2010). Modern sediment dispersal and accumulation on the outer
344 Poverty continental margin. *Marine Geology*, 270, 213–226. doi:10.1016/j.margeo.2009.10.015
345
- 346 Alonso, B., Ercilla, G., Casas, D., Stow, D.A.V., Rodriguez-Tovar, F. J., Dorador, J., & Hernandez-Molina, F.-J.
347 (2016). Contourite vs gravity-flow deposits of the Pleistocene Faro Drift (Gulf of Cadiz): Sedimentological and
348 mineralogical approaches. *Marine Geology*, 377, 77–94. <http://dx.doi.org/10.1016/j.margeo.2015.12.016>
349
- 350 Baeten, N. J., Laberg, J. S., Vanneste, M., Forsberg, C. F., Kvalstad, T. J., Forwick, M., Vorren, T. O., &
351 Hafildason, H. (2014). Origin of shallow submarine mass movements and their glide planes – Sedimentological and
352 geotechnical analyses from the continental slope off northern Norway. *Journal of Geophysical Research, Earth*
353 *Surface*, 119. doi:10.1002/2013JF003068
354
- 355 Bailey, W. S., McArthur, A. D., & McCaffrey, W.D. (2020). Distribution of contourite drifts on convergent
356 margins: Examples from the Hikurangi subduction margin of New Zealand. *Sedimentology*, 67, 12779.
357 doi:10.1111/sed.12779
358
- 359 Bailey, W., McArthur, A., & McCaffrey, W. (2021). Sealing potential of contourites drifts in deep-water fold and
360 thrust belts: Examples from the Hikurangi Margin, New Zealand. *Marine Petroleum Geology*, 123, 104776.
361 <https://doi.org/10.1016/j.marpetgeo.2020.104776>
362

- 363 Barnes, P. M., Nicol, A., and Harrison, T. (2002). Late Cenozoic evolution and earthquake potential of an active
364 listric thrust complex above the Hikurangi subduction zone, New Zealand. *Geological Society of America Bulletin*,
365 114(11), 1379–1405.
- 366
367 Barnes, P. M., Pecher, I., & LeVay, L. (2017). *Expedition 372 scientific prospectus: creeping gas hydrate slides and*
368 *LWD for Hikurangi subduction margin*. College Station, TX: International Ocean Discovery Program.
369 <http://dx.doi.org/10.14379/iodp.sp.372.2017>
- 370
371 Barnes, P. M., Pecher, I. A., LeVay, L. J., & 34 others (2019a). Site U1517. In I. A. Pecher, P. M. Barnes, L. J.
372 LeVay, Expedition 372A Scientists (Eds.), *Proceedings of the International Ocean Discovery Program* (Vol. 372A).
373 College Station, TX: International Ocean Discovery Program. <https://doi.org/10.14379/iodp.proc.372A.103.2019>
- 374
375 Barnes, P. M., Wallace, L. M., Saffer, D. M., Pecher, I. A., Petronotis, K. E., LeVay, L. J., and 55 others (2019b).
376 Site U1519. In L. M. Wallace, D. M. Saffer, P. M. Barnes, I. A. Pecher, K. E. Petronotis, L. J. LeVay, Expedition
377 372/375 Scientists (Eds.), *Hikurangi Subduction Margin Coring, Logging, and Observatories. Proceedings of the*
378 *International Ocean Discovery Program* (Vol. 372B/375). College Station, TX: International Ocean Discovery
379 Program. <https://doi.org/10.14379/iodp.proc.372B375.104.2019>
- 380
381 Bartetzko, A., & Kopf, A. J. (2007). The relationship of undrained shear strength and porosity with depth in shallow
382 (<50 m) marine sediments. *Sedimentary Geology*, 196, 235–249. doi:10.1016/j.sedgeo.2006.04.005
- 383
384 Biscaye, P. E. (1965). Mineralogy and sedimentation of recent deep-sea clay in the Atlantic Ocean and adjacent seas
385 and oceans. *Geological Society of America Bulletin*, 76, 803–832.
- 386
387 Bostock, H., Jenkins, C., Mackay, K., Carter, L., Nodder, S., & Orpin, A. (2018). Distribution of surficial sediments
388 in the ocean around New Zealand/Aotearoa. Part A: continental slope and deep ocean. *New Zealand Journal of*
389 *Geology and Geophysics*, 62(1), 1–23. <https://doi.org/10.1080/00288306.2018.1523198>
- 390
391 Bourget, J., Zaragosi, S., Ellouz-Zimmermann, N., Mouchot, N., Garlan, T., Schneider, J.-L., Lanfumey, V., &
392 Lallemand, S. (2011). Turbidite system architecture and sedimentary processes along topographically complex
393 slopes: the Makran convergent margin. *Sedimentology*, 58, 376–406. doi:10.1111/j.1365-3091.2010.01168.x
- 394
395 Brothers, R. N., & DeLaloye, M. (1982). Obducted ophiolites of North Island, New Zealand: origin, age,
396 emplacement and tectonic implications for Tertiary and Quaternary volcanicity. *New Zealand Journal of Geology*
397 *and Geophysics*, 25, 257–274.
- 398
399 Browne, G.H. (2004). Late Neogene sedimentation adjacent to the tectonically evolving North Island axial ranges:
400 insights from Kuripapango, western Hawke's Bay. *New Zealand Journal of Geology and Geophysics*, 47, 663–674.
- 401
402 Carter, L., & McCave, I. N. (1997). The sedimentary regime beneath the Deep Western Boundary Current inflow to
403 the southwest Pacific Ocean. *Journal of Sedimentary Research*, 67(6), 1005–1017.
- 404
405 Carter, L., & McCave, I. N. (2002). Eastern New Zealand drifts, Miocene-Recent. In D. A. V. Stow, C. J. Pudsey, J.
406 A. Howe, J.-C. Faugeres, A. R. Viana (Eds.), *Deep-water contourite systems: Modern drifts and ancient series,*
407 *seismic and sedimentary characteristics* (Memoir 22, pp. 385–407). London, Geological Society.
- 408
409 Carter, L., & Wilkin, J. (1999). Abyssal circulation around New Zealand – a comparison between observations and a
410 global circulation model. *Marine Geology*, 159, 221–239.
- 411
412 Carter, L., Carter, R. M., & McCave, I. N. (2004). Evolution of the sedimentary system beneath the deep Pacific
413 inflow off eastern New Zealand. *Marine Geology*, 205, 9–27. doi:10.1016/S0025-3227(04)00016-7
- 414
415 Chiswell, S. M. (2000). The Wairarapa Coastal Current. *New Zealand Journal of Marine and Freshwater Research*,
416 34, 303–315.
- 417
418 Chiswell, S. M. (2005). Mean and variability in the Wairarapa and Hikurangi Eddies, New Zealand. *New Zealand*

- 419 *Journal of Marine and Freshwater Research*, 39, 121–134.
420
- 421 Chiswell, S. M., & Roemmich, D. (1998). The East Cape Current and two eddies: a mechanism for larval retention?
422 *New Zealand Journal of Marine and Freshwater Research*, 32, 385–397.
423
- 424 Chiswell, S. M., Bostock, H. C., Sutton, P. J. H., & Williams, J. M. (2015). Physical oceanography of the deep seas
425 around New Zealand: a review. *New Zealand Journal of Marine and Freshwater Research*, 49(2), 286–317.
426 doi:10.1080/00288330.2014.992919
427
- 428 Claridge, G. G. C. (1960). Clay minerals, accelerated erosion, and sedimentation in the Waipaoa River catchment.
429 *New Zealand Journal of Geology and Geophysics*, 3, 184–191.
430
- 431 Cluzel, D., Black, P. M., Picard, C., & Nicholson, K. N. (2010). Geochemistry and tectonic setting of Matakaoa
432 Volcanics, East Coast Allochthon, New Zealand: Suprasubduction zone affinity, regional correlations, and origin.
433 *Tectonics*, 29, TC2013. doi:10.1029/2009TC002454
434
- 435 Cole, J. W., Deering, C. D., Burt, R. M., Sewell, S., Shane, P. A. R., & Matthews, N. E. (2014). Okataina Volcanic
436 Center, Taupo Volcanic Zone, New Zealand: A review of volcanism and synchronous pluton development in a
437 active, dominantly silicic caldera system. *Earth Science Reviews*, 128, 1–17.
438 <http://dx.doi.org/10.1016/j.earscirev.2013.10.008>
439
- 440 Collot, J.-Y., Lewis, K., Lamarche, G., & Lallemand, S. (2001). The giant Ruatoria debris avalanche on the northern
441 Hikurangi margin, New Zealand: Result of oblique seamount subduction. *Journal of Geophysical Research*,
442 106(B9), 19,271–19,297.
443
- 444 Contardo, X., Cembrano, J., Jensen, A., & Diaz-Naveas, J. (2008). Tectono-sedimentary evolution of marine slope
445 basins in the Chilean forearc (33°30'–36°50'S): Insights into their link with the subduction process. *Tectonophysics*,
446 459, 206–218. doi:10.1016/j.tecto.2007.12.014
447
- 448 Contardo, X. J., Kukowski, N., & Cembrano, J. M. (2011). Material transfer and its influence on the formation of
449 slope basins along the South Central Chilean convergent margin: Insights from scaled sandbox experiments.
450 *Tectonophysics*, 513, 20–36. doi:10.1016/j.tecto.2011.09.016
451
- 452 Couvin, B., Georgiopoulou, A., Mountjoy, J. J., Amy, L., Crutchley, G. J., Brunet, M., et al. (2020). A new
453 depositional model for the Tuaheni Landslide Complex, Hikurangi margin, New Zealand. In A. Georgiopoulou et
454 al. (Eds.). *Subaqueous mass movements and their consequences: Advances in process understanding, monitoring
455 and hazard assessments, Special Publication* (Vol. 500, pp. 551–566). London, Geological Society.
456 <https://doi.org/10.1144/SP500-2019-180>
457
- 458 Cronin, S. J., Neall, V. E., Lecointre, J. A., & Palmer, A. S. (1999). Dynamic interactions between lahars and stream
459 flow: A case study from Ruapehu volcano, New Zealand. *Geological Society of America Bulletin*, 111(1), 28–38.
460
- 461 Crutchley, G. J., Geiger, S., Pecher, I. A., Gorman, A. R., Zhu, H., & Henrys, S. A. (2010). The potential influence
462 of shallow gas and gas hydrates on seafloor erosion of Rock Garden, an uplifted ridge offshore of New Zealand.
463 *Geo-Marine Letters*, 30, 283–303. doi:10.1007/s00367-010-0186-y
464
- 465 Crutchley, G. J., Elger, J., Kuhlmann, J., Mountjoy, J. J., Orpin, A., Georgiopoulou, A., et al. (2022). Investigating
466 the basal shear zone of the submarine Tuaheni landslide complex, New Zealand: A core-log-seismic integration
467 study. *Journal of Geophysical Research: Solid Earth*, 127, e2021JB021997. <https://doi.org/10.1029/2021JB021997>
468
- 469 Cubrinovski, M., Bradley, B. A., Wentz, F., & Balachandra, A. (2022). Re-evaluation of New Zealand seismic
470 hazard for geotechnical assessment and design. *Bulletin New Zealand Society for Earthquake Engineering*, 55(1), 1–
471 14.
472

- 473 de Castro, S., Hernandez-Molina, F. J., de Weger, W., Jimenez-Espejo, F. J., Rodriguez-Tovar, F. J., Mena, A.,
474 Llave, E., & Sierro, F. J. (2020). Contourite characterization and its discrimination from other deep-water deposits in
475 the Gulf of Cadiz contourite depositional system. *Sedimentology*. doi:10.1111/sed.12813
476
- 477 Ding, F., Spiess, V., Fekete, N., Murton, B., Bruning, M., & Bohrmann, G. (2010). Interaction between accretionary
478 thrust faulting and slope sedimentation at the frontal Makran accretionary prism and its implications for hydrocarbon
479 seepage. *Journal of Geophysical Research*, 115, B08106. doi:10.1029/2008JB006246
480
- 481 Downs, D. T., Wilson, C. J. N., Cole, J. W., Rowland, J. V., Calvert, A. T., Leonard, G. S., & Keall, J. M. (2014).
482 Age and eruptive center of the Paeroa Subgroup ignimbrites (Whakamaru Group) within the Taupo Volcanic Zone
483 of New Zealand. *Geological Society of America Bulletin*, 126(9/10), 1131–1144. doi:10.1130/B30891.1
484
- 485 Dowrick, D. J., & Rhoades, D. A. (1998). Magnitudes of New Zealand earthquakes, 1901–1993. *Bulletin New
486 Zealand National Society for Earthquake Engineering*, 31(4), 260–280.
487
- 488 Ellis, S., Pecher, I., Kukowski, N., Xu, W., Henrys, S., & Greinert, J. (2010). Testing proposed mechanisms for
489 seafloor weakening at the top of gas hydrate stability on an uplifted submarine ridge (Rock Garden), New Zealand.
490 *Marine Geology*, 272, 127–140. doi:10.1016/j.margeo.2009.10.008
491
- 492 Erdman, C.F., & Kelsey, H. M. (1992). Pliocene and Pleistocene stratigraphy and tectonics, Ohara Depression and
493 Wakarara Range, North Island, *New Zealand Journal of Geology and Geophysics*, 35, 177–192.
494
- 495 Fagel, N. (2007). Clay minerals, deep circulation and climate. In C. Hillaire-Marcel & A. De Vernal (Eds.), *Proxies
496 in Late Cenozoic Paleoceanography* (pp. 139–184). Amsterdam, Elsevier.
497
- 498 Faure, K., Greinert, J., Pecher, I. A., Graham, I. J., Massoth, G. J., de Ronde, C. E., Wright, I. C., Baker, E. T., &
499 Olson, E. J. (2006). Methane seepage and its relation to slumping and gas hydrate at the Hikurangi margin, New
500 Zealand. *New Zealand Journal of Geology and Geophysics*, 49, 503–516.
501
- 502 Foster, G., & Carter, L. (1997). Mud sedimentation on the continental shelf at an accretionary margin – Poverty Bay,
503 New Zealand. *New Zealand Journal of Geology and Geophysics*, 40, 157–173.
504
- 505 Gatter, R., Clare, M. A., Hunt, J. E., Watts, M., Madhusudhan, B. N., Tailing, P. J., & Huhn, K. (2020). A multi-
506 disciplinary investigation of the AFEN Slide: the relationship between contourites and submarine landslides. In A.
507 Georgiopoulous et al. (Eds.). *Subaqueous mass movements and their consequences: Advances in process
508 understanding, monitoring and hazard assessments, Special Publication* (Vol. 500, pp. 173–193). London,
509 Geological Society. <https://doi.org/10.1144/SP500-2019-184>
510
- 511 Gatter, R., Clare, M. A., Kuhlmann, J., & Huhn, K. (2021). Characterization of weak layers, physical controls on
512 their global distribution and their role in submarine landslide formation. *Earth Science Reviews*, 223, 103845.
513 <https://doi.org/10.1016/j.earthscirev.2021.103845>
514
- 515 Ghisetti, F. C., Barnes, P. M., Ellis, S., Piazza-Faverola, A. A., & Barker, D. H. N. (2016). The last 2 Myr of
516 accretionary wedge construction in the central Hikurangi margin (North Island, New Zealand): Insights from
517 structural modeling. *Geochemistry Geophysics Geosystems*, 17, 2661–2686. doi:10.1002/2016GC006341
518
- 519 Gorsline, D. S. (1984). A review of fine-grained sediment origins, characteristics, transport, and deposition. In D. A.
520 V. Stow & D. J. W. Piper (Eds.), *Fine-grained sediments: Deep-water processes and facies. Special Publication*
521 (Vol. 15, pp. 17–34). London, Geological Society.
522
- 523 Gravley, D. M., Deering, C. D., Leonard, G. S., & Rowland, J. V. (2016). Ignimbrite flare-ups and their drivers: A
524 New Zealand perspective. *Earth Science Reviews*, 162, 65–82. <http://dx.doi.org/10.1016/j.earscirev.2016.09.007>
525
- 526 Gross, F., Mountjoy, J. J., Crutchley, G. J., Bottner, C., Koch, S., Bialas, J., et al. (2018). Free gas distribution and
527 basal shear zone development in a subaqueous landslide – Insight from 3D seismic imaging of the Tuaheni

- 528 Landslide Complex, New Zealand. *Earth and Planetary Science Letters*, 502, 231–243.
 529 <https://doi.org/10.1016/j.epsl.2018.09.002>
 530
- 531 Hampton, M. A., Lee, H. J., & Locat, J. (1996). Submarine landslides. *Reviews in Geophysics*, 34(1), 33–59.
 532
- 533 Harders, R., Kutterolf, S., Hensen, C., Moerz, T., & Brueckman, W. (2010). Tephra layers: A controlling factor on
 534 submarine translational sliding? *Geochemistry Geophysics Geosystems*, 11(5), Q05S23.
 535 doi:10.1029/2009GC002844
 536
- 537 Harders, R., Ranero, C. R., Weinrebe, W., & Behrmann, J. H. (2011). Submarine slope failures along the convergent
 538 continental margin of the Middle America Trench. *Geochemistry Geophysics Geosystems*, 12(6), Q05S32.
 539 doi:10.1029/2010GC003401
 540
- 541 Heap, M. J., Gravley, D. M., Kennedy, B. M., Gilg, H. A., Bertolett, E., & Barker, S. L. L. (2020). Quantifying the
 542 role of hydrothermal alteration in creating geothermal and epithermal mineral resources: The Okakuri ignimbrite
 543 (Taupo Volcanic Zone, New Zealand). *Journal of Volcanology and Geothermal Research*, 390, 106703.
 544 <https://doi.org/10.1016/j.volgeores.2019.106703>
 545
- 546 Hein, J. R., & Scholl, D. W. (1978). Diagenesis and distribution of late Cenozoic volcanic sediment in the southern
 547 Bering Sea. *Geological Society of America Bulletin*, 89(2), 197–210.
 548
- 549 Hicks, D. M., Shankar, U., McKerchar, A. I., Basher, L., Lynn, I., Page, M., & Jessen, M. (2011). Suspended
 550 sediment yields from New Zealand rivers. *Journal of Hydrology*, 50(1), 81–142.
 551
- 552 Hidgson, K. A., & Manville, V. R. (1999). Sedimentology and flow behavior of a rain-triggered lahar,
 553 Mangatoetoe Stream, Ruapehu volcano, New Zealand. *Geological Society of America Bulletin*, 111(5), 743–754.
 554
- 555 Hill, J. C., Watt, J. T., Brothers, D. S., & Kluesner, J. W. (2020). Submarine canyons, slope failures and mass
 556 transport processes in southern Cascadia. In A. Georgiopoulous et al. (Eds.). *Subaqueous mass movements and their
 557 consequences: Advances in process understanding, monitoring and hazard assessments, Special Publication* (Vol.
 558 500, pp. 453–475). London, Geological Society. <https://doi.org/10.1144/SP500-2019-169>
 559
- 560 Hocking, M. W. A., Hannington, M. D., Percival, J. B., Stoffers, P., Schwarz-Schampera, U., & de Ronde, C. E. J.
 561 (2010). Clay alteration of volcanoclastic material in a submarine geothermal system, Bay of Plenty, New Zealand.
 562 *Journal of Volcanology and Geothermal Research*, 191, 180–192. doi:10.1016/j.volgeores.2010.01.018
 563
- 564 Huff, W. D. (2016). K-bentonites: A review. *American Mineralogist*, 101, 43–70. [http://dx.doi.org/10.2138/am-](http://dx.doi.org/10.2138/am-2016-5339)
 565 [2016-5339](http://dx.doi.org/10.2138/am-2016-5339)
 566
- 567 Ikari, M. J., Saffer, D. M., & Marone, C. (2007). Effect of hydration state on the frictional properties of
 568 montmorillonite-based fault gouge. *Journal of Geophysical Research*, 112, B06423. doi:10.1029/2006JB004748
 569
- 570 Ikari, M. J., Strasser, M., Saffer, D. M., & Kopf, A. J. (2011). Submarine landslide potential near the megasplay
 571 fault at the Nankai subduction zone. *Earth and Planetary Science Letters*, 312, 453–462.
 572 doi:10.1016/j.epsl.2011.10.024
 573
- 574 Ikari, M. J., Kopf, A. J., Hupers, A., & Vogt, C. (2018). Lithologic controls on frictional strength variations in
 575 subduction zone sediment inputs. *Geosphere*, 14(2), 604–625. doi:10.1130/GES01546.1
 576
- 577 Iso, N., Okada, A., Ota, Y., & Yoshikawa, T. (1982). Fission-track ages of late Pleistocene tephra on the Bay of
 578 Plenty coast, North Island, New Zealand. *New Zealand Journal of Geology and Geophysics*, 25, 295–303.
 579
- 580 Jiao, R., Seward, D., Little, T. A., & Kohn, B. P. (2014). Thermal history and exhumation of basement rocks from
 581 Mesozoic to Cenozoic subduction cycles, central North Island, New Zealand. *Tectonics*, 33, 1920–1935.
 582 doi:10.1002/2014TC003653
 583

- 584 Kock, I., & Huhn, K. (2007). Influence of particle shape on the frictional strength of sediments – A numerical case
585 study. *Sedimentary Geology*, 196, 217–233. doi:10.1016/j.sedgeo.2006.07.011
586
- 587 Kohn, B. P., & Topping, W. W. (1978). Time-space relationships between late Quaternary rhyolitic and andesitic
588 volcanism in the southern Taupo volcanic zone, New Zealand. *Geological Society of America Bulletin*, 89(8), 1265–
589 1271.
590
- 591 Kremer, K., Usman, M. O., Satoguchi, Y., Nagahashi, Y., Vadkkepuliambatta, S., Panieri, G., & Strasser, M.,
592 (2017). Possible climate preconditioning on submarine landslides along a convergent margin, Nankai Trough (NE
593 Pacific). *Progress in Earth and Planetary Science*, 4, 20. doi:10.1186/s40645-017-0134-9
594
- 595 Kuhlman, J., Huhn, K., & Ikari, M. J., (2016). Do embedded volcanoclastic layers serve as potential glide planes?:
596 An integrated analysis from the Gela Basin offshore southern Sicily. In G. Lamarche, G., et al. (Eds.), *Submarine*
597 *mass movements and their consequences, advances in natural and technological hazards research* (Vol. 41, pp.
598 273–280). Switzerland, Springer International Publishing. doi:10.1007/978-3-319-20979-1_27
599
- 600 Kuhlmann, J., Orpin, A. R., Mountjoy, J. J., Crutchley, G. J., Henrys, S., Lunenburg, R., & Huhn, K. (2019).
601 Seismic and lithofacies characterization of a gravity core transect down the submarine Tuaheni Landslide Complex,
602 NE New Zealand. In D. G. Lintern (Eds.), *Subaqueous mass movements, Special Publications* (Vol. 477, pp. 479–
603 495). London, Geological Society. <https://doi.org/10.1144/SP477.37>
604
- 605 Laberg, J. S., Baeten, N. J., Vanneste, M., Forsberg, C. F., Forwick, M., & Haflidason, H. (2016). Sediment failure
606 affecting muddy contourites on the continental slope offshore northern Norway: Lessons learned and some
607 outstanding issues. In G. Lamarche et al. (Eds.), *Submarine mass movements and their consequences, Advances in*
608 *natural and technological hazards research* (Vol. 41, pp. 281–290). Switzerland, Springer International Publishing.
609 doi:10.1007/978-3-319-20979-1_28
610
- 611 Lewis, K. B., Lallemand, S. E., & Carter, L. (2004). Collapse in a Quaternary shelf basin off East Cape, New
612 Zealand: evidence for passage of a subducted seamount inboard of the Ruatoria giant avalanche. *New Zealand*
613 *Journal of Geology and Geophysics*, 47, 415–429.
614
- 615 Libbey, R. B., Longstaffe, F. J., & Flemming, R. L. (2013). Clay mineralogy, oxygen isotope geochemistry, and
616 water/rock ratio estimates, Te Mihi area, Wairakei geothermal field, New Zealand. *Clays and Clay Minerals*, 61(3),
617 204–217. doi:10.1346/CCMN.2013.0610304
618
- 619 Locat, J., & Lee, H. J. (2002). Submarine landslides: advances and challenges. *Canadian Geotechnical Journal*, 39,
620 193–212. doi:10.1139/T01-089
621
- 622 Locat, J., Leroueil, S., Locat, A., & Lee, H. (2014). Weak layers: Their definition and classification from a
623 geotechnical perspective. In S. Krastel et al. (Eds.), *Submarine mass movements and their consequences, advances*
624 *in natural and technological hazards research* (pp. 3–12). Switzerland, Springer International Publ.
625 doi:10.1007/978-3-319-00972-8_1
626
- 627 Logan, J. M., & Rauenzahn, K. A. (1987). Frictional dependence of gouge mixtures of quartz
628 and montmorillonite on velocity, composition and fabric. *Tectonophysics*, 144, 87–108.
629
- 630 Lowe, D. J., Blaauw, M., Hogg, A. G., & Newnham, R. M. (2013). Ages of 24 widespread tephras erupted since
631 30,000 years ago in New Zealand, with re-evaluation of the timing and palaeoclimatic implications of the
632 Lateglacial cool episode recorded at Kaipo bog. *Quaternary Science Reviews*, 74, 170–194.
633 <http://dx.doi.org/10.1016/j.quascirev.2012.11.022>
634
- 635 Luo, M., Torres, M. E., Kasten, S., & Mountjoy, J. J. (2020). Constraining the age and evolution of the Tuaheni
636 Landslide Complex, Hikurangi margin, New Zealand, using pore-water geochemistry and numerical modeling.
637 *Geophysical Research Letters*, 47, e2020GL087243. <https://doi.org/10.1029/2020GL087243>
638
- 639 Lupini, J. F., Skinner, A. E., & Vaughan, P. R. (1981). The drained residual strength of cohesive

- 640 soils. *Geotechnique*, 31, 181–213.
- 641
- 642 MacKinnon, T. C. (1983). Origin of Torlesse terrane and coeval rocks, South Island, New Zealand. *Geological*
643 *Society of America Bulletin*, 94, 967–985.
- 644
- 645 Maison, T., Potel, S., Malie, P., Ferreiro Mahlmann, R., Chanier, F., Mahieux, G., & Bailleul, J. (2018). Low-grade
646 evolution of clay minerals and organic matter in fault zones of the Hikurangi prism (New Zealand). *Clay Minerals*,
647 53, 579–602. <https://doi.org/10.1180/clm.2018.46>
- 648
- 649 Marden, M., Mazengarb, C., Palmer, A., Berryman, K., & Rowan, D. (2008). Last glacial aggradation and
650 postglacial sediment production from the non-glacial Waipaoa and Waimata catchments, Hikurangi margin, North
651 Island, New Zealand. *Geomorphology*, 99, 404–419. doi:10.1016/j.geomorph.2007.12.003
- 652
- 653 Marsaglia, K. M., DeVaughn, A. M., James, D. E., & Marden, M. (2010). Provenance of fluvial terrace sediments
654 within the Waipaoa sedimentary system and their importance to New Zealand source-to-sink studies. *Marine*
655 *Geology*, 270, 84–93. doi:10.1016/j.margeo.2009.10.017
- 656
- 657 Marsaglia, K. M., Mortimer, N., Bender-Whitaker, C., Marden, M., & Mazengarb, C. (2014). Ophiolitic
658 Ikingia igneous conglomerate (Early Miocene), North Island, New Zealand: evidence for an island source related to
659 subduction initiation and deposition within a slump-generated submarine slope re-entrant. *New Zealand Journal of*
660 *Geology and Geophysics*, 57(2), 219–235. <http://dx.doi.org/10.1080/00288306.2014.898665>
- 661
- 662 Masson, D. G., Harbitz, C. B., Wynn, R. B., Pedersen, G., & Lovholt, F. (2006). Submarine landslides: processes,
663 triggers and hazard prediction. *Philosophical Transactions Royal Society A*, 364, 2009–2039.
664 doi:10.1098/rsta.2006.1810
- 665
- 666 McAdoo, B. G., Capone, M. K., & Minder, J. (2004). Seafloor geomorphology of convergent margins: Implications
667 for Cascadia seismic hazard. *Tectonics*, 23, TC6008. doi:10.1029/2003TC001570
- 668
- 669 McArthur, A. D., Claussmann, B., Bailleul, J., Clare, A., & McCaffrey, W. D. (2020). Variation in syn-subduction
670 sedimentation patterns from inner to outer portions of deep-water fold and thrust belts: examples from the Hikurangi
671 subduction margin of New Zealand. In J. A. Hammerstein, R. DiCuia, M. A. Cottam, G. Zamora, & R. W. H. Butler
672 (Eds.), *Fold and thrust belts: structural style, evolution and exploration, Special Publication* (Vol. 490, pp. 285–
673 310). London, Geological Society. <https://doi.org/10.1144/SP490-2018-95>
- 674
- 675 McCave, I. N. (1984). Erosion, transport and deposition of fine-grained marine sediments. In D. A. V. Stow & D. J.
676 W. Piper (Eds.), *Fine-grained sediments: Deep-water processes and facies. Special Publication* (Vol. 15, pp. 35–
677 70). London, Geological Society.
- 678
- 679 Micallef, A., Mountjoy, J.J., Krastel, S., Crutchley, G., & Koch, S. (2015). Shallow gas and the development of a
680 weak layer in submarine spreading, Hikurangi margin (New Zealand). In G. Lamarche et al. (Eds.), *Submarine mass*
681 *movements and their Consequences, advances in natural and technological hazards research* (Vol. 41, pp. 419–
682 426). Switzerland, Springer International Publ. doi:10.1007/978-3-319-20979-1_42
- 683
- 684 Miramontes, E., Garziglia, S., Sultan, N., Jouet, G., & Cattaneo, A. (2018). Morphological control of slope
685 instability in contourites: a geotechnical approach. *Landslides*, 15, 1085–1095. doi:10.1007/s10346-018-0956-6
- 686
- 687 Miramontes, E., Sultan, N., Garziglia, S., Joulet, G., Pelleter, E., & Cattaneo, A. (2018). Altered volcanic deposits as
688 basal failure surfaces of submarine landslides. *Geology*, 46(7), 663–666. <https://doi.org/10.1130/G40268>
- 689
- 690 Moore, D. M., & Reynolds, R. C., Jr. (1989). Sample preparation techniques for clay minerals. In D. M. Moore & R.
691 C. Reynolds, Jr. (Eds.), *X-ray diffraction and the identification and analysis of clay minerals* (pp. 179–201). New
692 York, Oxford University Press.
- 693
- 694 Moore, G. F., & Karig, D. E. (1976). Development of sedimentary basins on the lower trench slope. *Geology*, 4,
695 693–697.

- 696
697 Mountjoy, J. J., Barnes, P. M., & Pettinga, J. R. (2009a). Morphostructure and evolution of submarine canyons
698 across an active margin: Cook Strait sector of the Hikurangi margin, New Zealand. *Marine Geology*, 260, 45–68.
699 doi:10.1016/j.margeo.2009.01.006
700
- 701 Mountjoy, J. J., McKean, J., Barnes, P. M., & Pettinga, J. R. (2009b). Terrestrial-style slow-moving earthflow
702 kinematics in a submarine landslide complex. *Marine Geology*, 267, 114–127. doi:10.1016/j.margeo.2009.09.007
703
- 704 Mountjoy, J. J., Micallef, A., Stevens, C. L., & Stirling, M. W. (2014a). Holocene sedimentary activity in a non-
705 terrestrially coupled submarine canyon: Cook Strait Canyon system, New Zealand. *Deep-Sea Research II*, 104, 120–
706 133. <http://dx.doi.org/10.1016/j.dsr2.2013.09.001>
707
- 708 Mountjoy, J. J., Pecher, I., Henrys, S., Crutchley, G., Barnes, P. M., & Plaza-Faverola, A. (2014b). Shallow methane
709 hydrate system controls ongoing, downslope sediment transport in a low-velocity active submarine landslide
710 complex, Hikurangi margin, New Zealand. *Geochemistry Geophysics Geosystems*, 15, 4137–4156.
711 doi:10.1002/2014GC005379
712
- 713 Mountjoy, J. J., Georgiopoulou, A., Chaytor, J., Clare, M. A., Gamboa, D., & Moernaut, J. (2020). Subaqueous
714 mass movements in the context of observations of contemporary slope failure. In: A. Georgiopoulou et al. (Eds.),
715 *Subaqueous mass movements and their consequences: Advances in process understanding, monitoring and hazard*
716 *assessments, Special Publications* (Vol. 500, pp. 1–12). London, Geological Society. [https://doi.org/10.1144/SP500-](https://doi.org/10.1144/SP500-2019-237)
717 [2019-237](https://doi.org/10.1144/SP500-2019-237)
718
- 719 Muck, M. T., & Underwood, M. B. (1990). Upslope flow of turbidity currents: A comparison among field
720 observations, theory, and laboratory models. *Geology*, 18, 54–57.
721
- 722 Nakamura, S., Gibo, S., Egashira, K., & Kimura, S. (2010). Platy layer silicate minerals for controlling residual
723 strength in landslide soils of different origins and geology. *Geology*, 38(8), 743–746. doi:10.1130/G30908.1
724
- 725 Neef, G. (1999). Neogene development of the onland part of the forearc in northern Wairarapa, North Island, New
726 Zealand: a synthesis. *New Zealand Journal of Geology and Geophysics*, 42, 113–135.
727
- 728 Nelson, C. H., Escutia, C., Damuth, J. E., & Twichell, D. C., Jr. (2011). Interplay of mass-transport and turbidite-
729 system deposits in different active tectonic and passive continental margin settings: External and local controlling
730 factors. In R. C. Shipp, P. Weimer, & H. W. Posamentier (Eds.), *Mass-transport deposits in deepwater settings,*
731 *Special Publication* (Vol. 96). Society for Sedimentary Geology. <https://doi.org/10.2110/sepmssp.096.039>
732
- 733 Nishida, N. (2016). Microstructure of muddy contourites from the Gulf of Cadiz. *Marine Geology*, 377, 110–117.
734 <http://dx.doi.org/10.1016/j.margeo.2015.08.017>
735
- 736 Officer, S. J., Tillman, R. W., Palmer, A. S., & Whitton, J. S. (2006). Variability of clay mineralogy in two New
737 Zealand steep-land topsoils under pasture. *Geoderma*, 132, 427–440. doi:10.1016/j.geoderma.2004.11.027
738
- 739 Orpin, A. R. (2004). Holocene sediment deposition on the Poverty-slope margin by the muddy Waipaoa River, East
740 Coast New Zealand. *Marine Geology*, 209, 69–90. doi:10.1016/j.margeo.2004.06.001
741
- 742 Paquet, F., Proust, J.-N., Barnes, P. M., & Pettinga, J. R. (2009). Inner-forearc sequence architecture in response to
743 climatic and tectonic forcing since 150 ka: Hawke's Bay, New Zealand. *Journal of Sedimentary Research*, 79, 97–
744 124. doi:10.2110/jsr.2009.019
745
- 746 Pedley, K. L., Barnes, P. M., Pettinga, J. R., & Lewis, K. B. (2010). Seafloor structural geomorphic evolution of the
747 accretionary frontal wedge in response to seamount subduction, Poverty Indentation, New Zealand. *Marine*
748 *Geology*, 270, 119–138. doi:10.1016/j.margeo.2009.11.006
749
- 750 Piper, D. J. W., von Huene, R., & Duncan, J. R. (1973). Late Quaternary sedimentation in the active eastern
751 Aleutian Trench. *Geology*, 1(1), 19–22.

- 752
753 Poudroux, H., Proust, J.-N., Lamarche, G., Orpin, A., & Neil, H. (2012). Postglacial (after 18 ka) deep-sea
754 sedimentation along the Hikurangi subduction margin (New Zealand): Characterisation, timing and origin of
755 turbidites. *Marine Geology*, 295–298, 51–76. doi:10.1016/j.margeo.2011.11.002
756
- 757 Prieto, M. L., Moscardelli, L., & Wood, L. J. (2016). Exploring the influence of deepwater currents as potential
758 triggers for slope instability. In G. Lamarche et al. (Eds.), *Submarine mass movements and their consequences*,
759 *Advances in natural and technological hazards research* (Vol. 41, pp. 331–340). Switzerland, Springer International
760 Publishing. doi:10.1007/978-3-319-20979-1_33
761
- 762 Procter, J. N., Cronin, S. J., Zernack, A. V., Lube, G., Stewart, R. B., Nemeth, K., & Keys, H. (2014). Debris flow
763 evolution and the activation of an explosive hydrothermal system; Te Maari, Tongariro, New Zealand. *Journal of*
764 *Volcanology and Geothermal Research*, 286, 303–316. <http://dx.doi.org/10.1016/j.volgeores.2014.07.006>
765
- 766 Reid, C. M. (1998). Stratigraphy, paleontology, and tectonics of lower Miocene rocks in the Waipatik/Mangatuna
767 area, southern Hawke's Bay, New Zealand. *New Zealand Journal of Geology and Geophysics*, 41, 115–131.
768
- 769 Rodriguez-Tovar, F. J., & Hernandez-Molina, F. J. (2018). Ichnological analysis of contourites: Past, present and
770 future. *Earth Science Reviews*. <https://doi.org/10.1016/j.earscirev.2018.05.008>
771
- 772 Saffer, D. M., Wallace, L. M., Barnes, P. M., Pecher, I. A., Petronotis, K. E., LeVay, L. J., and 55 others (2019).
773 Expedition 372B/375 summary. In L. M. Wallace, D. M. Saffer, P. M. Barnes, I. A. Pecher, K. E. Petronotis, L. J.
774 LeVay, Expedition 372/375 Scientists (Eds.), *Hikurangi subduction margin coring, logging, and observatories*,
775 *Proceedings of the International Ocean Discovery Program* (Vol. 372B/375). College Station, TX, International
776 Ocean Discovery Program. <https://doi.org/10.14379/iodp.proc.372B375.101.2019>
777
- 778 Screamon, E. J., Torres, M. E., Dugan, B., Heeschen, K. U., Mountjoy, J. J., Ayres, C., et al. (2019). Sedimentation
779 controls on methane-hydrate dynamics across glacial/interglacial stages: An example from International Ocean
780 Discovery Program Site U1517, Hikurangi margin. *Geochemistry Geophysics Geosystems*, 20.
781 <https://doi.org/10.1029/2019GC008603>
782
- 783 Shimamoto, T., & J. M. Logan (1981). Effects of simulated clay gouges on the sliding behavior of Tennessee
784 sandstone. *Tectonophysics*, 75, 243–255.
785
- 786 Silver, M. M. W., & Dugan, B. (2020). The influence of clay content on submarine slope failure: insights from
787 laboratory experiments and numerical models. In A. Georgiopoulous et al. (Eds.), *Subaqueous mass movements and*
788 *their consequences: Advances in process understanding, monitoring and hazard assessments. Special Publication*
789 (Vol. 500, pp. 301–309). London, Geological Society. <https://doi.org/10.1144/SP500-2019-186>
790
- 791 Simpson, M. P., Gazley, M. F., Stuart, A. G. J., Pearce, M. A., Birchall, R., Chappell, D., et al. (2019).
792 Hydrothermal alteration at the Karangahake epithermal Au-Ag deposit, Hauraki goldfield, New Zealand. *Economic*
793 *Geology*, 114(2), 243–273. doi:10.5382/econgeo.2019.4630
794
- 795 Sporli, K. B. (1979). Mesozoic tectonics, North Island, New Zealand. *Geological Society of America Bulletin*, 89,
796 415–425.
797
- 798 Stegmann, S., Strasser, M., Anselmetti, F., & Kopf, A. (2007). Geotechnical in situ characterization of subaquatic
799 slopes: The role of pore pressure transients versus frictional strength in landslide initiation. *Geophysical Research*
800 *Letters*, 34, L07607. doi:10.1029/2006GL029112
801
- 802 Stoecklin, A., Friedli, B., & Puzrin, A. M. (2017). Sedimentation as a control for large submarine landslides:
803 Mechanical modeling and analysis of the Santa Barbara Basin. *Journal of Geophysical Research: Solid Earth*, 122,
804 8645–8663. <https://doi.org/10.1002/2017JB014752>
805
- 806 Stow, D., & Smillie, Z. (2020). Distinguishing between deep-water sediment facies: turbidites, contourites and
807 hemipelagites. *Geosciences*, 10, 68. doi:10.3390/geosciences10020068

- 808
809 Stow, D. A., Faugeres, J. C., Howe, J. A., Pudsey, C. J., & Viana, A. R. (2002). Bottom currents, contourites and
810 deep-sea sediment drifts: current state-of-the-art. *Geological Society of London Memoir*, 22, 7–20.
811
- 812 Sultan, N., Cochonat, P., Canals, M., Cattaneo, A., Dennielou, B., Haflidason, H., et al. (2004). Triggering
813 mechanisms of slope instability processes and sediment failures on continental margins: a geotechnical approach.
814 *Marine Geology*, 213, 291–321. doi:10.1016/j.margeo.2004.10.011
815
- 816 Takahashi, M., Azuma, S., Ito, H., Kanagawa, K., & Inoue, A. (2014). Frictional properties of the shallow Nankai
817 Trough accretionary sediments dependent on the content of clay minerals. *Earth Planets Space*, 66, 75.
818 <http://www.earth-planets-space.com/content/66/1/75>
819
- 820 Tembe, S., Lockner, D. A., & Wong, T.-F. (2010). Effect of clay content and mineralogy on frictional sliding
821 behavior of simulated gouges: Binary and ternary mixtures of quartz, illite, and montmorillonite. *Journal of*
822 *Geophysical Research*, 115, B03416. doi:10.1029/2009JB006383
823
- 824 Tiwari, B., & Marui, H. (2005). A new method for the correlation of residual shear strength of the soil with
825 mineralogical composition. *Journal of Geotechnical and Geoenvironmental Engineering*, 131(9), 1139–1150.
826 doi:10.1061/(ASCE)1090-0241(2005)131:9(1139)
827
- 828 Thornburg, T. M., & Kulm, L. D. (1987). Sedimentation in the Chile Trench: Depositional morphologies,
829 lithofacies, and stratigraphy. *Geological Society of America Bulletin*, 98(1), 33–52.
830
- 831 Trütner, S., Hüpers, A., Ikari, M. J., Yamaguchi, A., & Kopf, A. J. (2015). Lithification facilitates frictional
832 instability in argillaceous subduction zone sediments. *Tectonophysics*, 665, 177–185.
833 <http://dx.doi.org/10.1016/j.tecto.2015.10.004>
834
- 835 Underwood, M. B. (2020). Data report: reconnaissance of bulk sediment composition and clay mineral assemblages:
836 inputs to the Hikurangi subduction system. In L. M. Wallace, D. M. Saffer, P. M. Barnes, I. A. Pecher, K. E.
837 Petronotis, L. J. LeVay, Expedition 372/375 Scientists (Eds.), *Hikurangi subduction margin coring, logging, and*
838 *observatories, Proceedings of the International Ocean Discovery Program* (Vol. 372B/375). College Station, TX,
839 International Ocean Discovery Program. <https://doi.org/10.14379/iodp.proc.372B375.203.2020>
840
- 841 Underwood, M. B. (2022). Data report. Clay mineral assemblages within Hikurangi trench-slope deposits, IODP
842 Expedition 372B/375 Site U1519, offshore New Zealand. In L. M. Wallace, D. M. Saffer, P. M. Barnes, I. A.
843 Pecher, K. E. Petronotis, L. J. LeVay, Expedition 372/375 Scientists (Eds.), *Hikurangi subduction margin coring,*
844 *logging, and observatories, Proceedings of the International Ocean Discovery Program* (Vol. 372B/375). College
845 Station, TX, International Ocean Discovery Program. <https://doi.org/10.14379/iodp.proc.372B375.209.2022>
846
- 847 Underwood, M. B., & Bachman, S. B. (1982). Sedimentary facies associations within subduction complexes. In J.
848 K. Leggett (Ed.), *Trench-forearc geology, Special Publication* (Vol. 10, pp. 537–550). London, Geological Society.
849
- 850 Underwood, M. B., & Moore, G.F. (1995). Trenches and trench-slope basins. In C. J. Busby, R. V. Ingersoll (Eds.),
851 *Tectonics of Sedimentary Basins* (pp. 179–21). Malden, MA, Blackwell Scientific.
852
- 853 Underwood, M. B., & Dugan, B. (2021). Data report: Clay mineral assemblages within and beneath the Tuaheni
854 landslide complex, IODP Expedition 372A Site U1517, offshore New Zealand. In I. A. Pecher, P. M. Barnes, L.J.
855 LeVay, and Expedition 372A Scientists (Eds.), *Creeping Gas Hydrate Slides. Proceedings of the International*
856 *Ocean Discovery Program* (Vol. 372A). College Station, TX, International Ocean Discovery Program.
857 <https://doi.org/10.14379/iodp.proc.372A.201.2021>
858
- 859 Underwood, M. B., Lawler, N., & McNamara, K. (2020). Data report: standard mineral mixtures, normalization
860 factors, and determination of error for quantitative X-ray diffraction analyses of bulk powders and clay-sized
861 mineral assemblages. In L. M. Wallace, D. M. Saffer, P. M. Barnes, I. A. Pecher, K. E. Petronotis, L. J. LeVay,
862 Expedition 372/375 Scientists (Eds.), *Hikurangi subduction margin coring, logging, and observatories, Proceedings*
863 *of the International Ocean Discovery Program* (Vol. 372B/375). College Station, TX, International Ocean

- 864 Discovery Program. <https://doi.org/10.14379/iodp.proc.372B375.201.2020>
865
- 866 Vandorpe, T., Collart, T., Cnudde, V., Lebreiro, S., Hernandez-Molina, F. J., Alonso, B., et al. (2019). Quantitative
867 characterization of contourite deposits using medical CT. *Marine Geology*, 417, 106003.
868 <https://doi.org/10.1016/j.margeo.2019.106003>
869
- 870 Vanneste, M., Sultan, N., Garziglia, S., Forsberg, C. F., & L'Heureux, J.-S. (2014). Seafloor instabilities and
871 sediment deformation processes: The need for integrated, multi-disciplinary investigations. *Marine Geology*, 152,
872 183–214. <http://dx.doi.org/10.1016/j.margeo.2014.01.005>
873
- 874 Warr, L. N., & Cox, S. C. (2016). Correlating illite (Kübler) and chlorite (Árakai) “crystallinity” indices with
875 metamorphic mineral zones of the South Island, New Zealand. *Applied Clay Science*, 134, 164–174.
876 <http://dx.doi.org/10.1016/j.clay.2016.06.024>.
877
- 878 Watson, S. J., Mountjoy, J. J., & Crutchley, G. J. (2020). Tectonic and geomorphic controls on the distribution of
879 submarine landslides across active and passive margins, eastern New Zealand. In A. Georgiopoulos et al. (Eds.).
880 *Subaqueous mass movements and their consequences: Advances in process understanding, monitoring and hazard*
881 *assessments, Special Publication* (Vol. 500, pp. 477–494). London, Geological Society.
882 <https://doi.org/10.1144/SP500-2019-165>
883
- 884 Wilson, C. J. N., & Rowland, J. V. (2016). The volcanic, magmatic and tectonic setting of the Taupo Volcanic Zone,
885 New Zealand, reviewed from a geothermal perspective. *Geothermics*, 59, 168–187.
886 <http://dx.doi.org/10.1016/j.geothermics.2015.06.013>
887
- 888 Yamada, Y., Yamashita, Y., & Yamamoto, Y. (2010). Submarine landslides at subduction margins: Insights from
889 physical models. *Tectonophysics*, 484, 156167. doi:10.1016/j.tecto.2009.09.007
890